Available online at www.sciencedirect.com
ScienceDirect
Magnetic Resonance Imaging xx (2008) xxx – xxx
MAGNETIC RESONANCE IMAGING

An optimized 3D inversion recovery prepared fast spoiled gradient recalled sequence for carotid plaque hemorrhage imaging at 3.0 T☆

David C. Zhu[a,b,c,*], Marina S. Ferguson[d], J. Kevin DeMarco[a]

[a]Department of Radiology, Michigan State University, East Lansing, MI 48824, USA
[b]Department of Psychology, Michigan State University, East Lansing, MI 48824, USA
[c]Cognitive Imaging Research Center, Michigan State University, East Lansing, MI 48824, USA
[d]Vascular Imaging Lab, University of Washington, Seattle, WA 98109, USA

Received 31 January 2008; revised 2 May 2008; accepted 2 May 2008

Abstract

An optimized 3D inversion recovery prepared fast spoiled gradient recalled sequence (IR FSPGR) on a 3-T scanner for carotid plaque imaging is described. It offers clear blood and fat signal suppression at the carotid artery bifurcation and highlights the regions of carotid plaque affected by hemorrhage at 3 T with high contrast and contrast-to-noise ratio compared with other sequences. It can potentially be used to replace the more traditional noncontrast T_1-weighted 2D black-blood imaging for hemorrhage detection and offers additional benefits of high-resolution 3D volumetric visualization.

Keywords: 3D IR FSPGR; Carotid plaque imaging

1. Introduction

In an effort to find clinically relevant markers of plaque vulnerability and thereby increased risk of subsequent stroke, a number of noninvasive imaging strategies have been investigated. Magnetic resonance imaging (MRI) shows promise for imaging the carotid artery lumen and at the same time provides detailed artery wall information [1]. Recent pathophysiological studies have centered on the identification and understanding of "vulnerable plaque" that poses an increased risk for thromboembolic event causing ischemia [2]. Based on the previous histopathological studies of carotid endarterectomy specimens, intraplaque hemorrhage into the carotid atherosclerotic plaque has been shown to create instability and progression as well as an association with current symptoms [3,4]. An MRI technique that can successfully detect intraplaque hemorrhage is important. Such a noninvasive evaluation of the in vivo appearance of carotid plaque would permit evaluation of the prospective importance of plaque hemorrhage to predict new ipsilateral carotid thromboembolic disease.

Previous experience at 1.5-T MR demonstrates that T_1-weighted black-blood images (T1WI) and 3D time-of-flight (TOF) MR angiogram (MRA) can detect intraplaque hemorrhage with good sensitivity and moderate specificity [5]. The in vivo appearance of carotid plaque hemorrhage could be further characterized as Type I or Type II based upon their appearance on T_2-weighted images [6]. The classification of hemorrhage type was shown to correlate with a history of recent ipsilateral carotid thromboembolic disease [7]. Moody et al. [8] also developed a T_1-weighted magnetization-prepared 3D gradient echo sequence to characterize the hemorrhagic carotid plaque at 1.5 T with a good sensitivity and specificity. We sought to extend in vivo carotid plaque imaging from 1.5 to 3 T. Previous work has demonstrated the improved contrast-to-noise ratio (CNR) at 3 T compared to 1.5 T [9]. We have developed an optimized 3D inversion recovery prepared fast spoiled gradient recalled sequence (IR FSPGR) with improved time efficiency over

☆ Grant support: The Core Analytical Facility Fund and an IRGP grant from Michigan State University, an extramural research grant from Bracco Diagnostic, Inc., and financial support from GE Healthcare Systems.

* Corresponding author. Michigan State University, East Lansing, MI 48824, USA. Tel.: +1 517 353 9432; fax: +1 517 353 3745.
E-mail address: zhuda@msu.edu (D.C. Zhu).

0730-725X/$ – see front matter © 2008 Elsevier Inc. All rights reserved.
doi:10.1016/j.mri.2008.05.002

the product sequence to allow high-resolution imaging of both carotid bifurcations under 5 min at 3 T. Intracranial hemorrhages demonstrate similar T_1 shortening characteristics on T_1-weighted brain images and T_2 decay enhancement on T_2-weighted images [10]. We hypothesized that exploiting both the presumed short T_1 values of plaque hemorrhage with the improved CNR at 3 T using the highly T_1-weighted contrast of the proposed 3D IR FSPGR would lead to higher CNR in regions of plaque hemorrhage compared with T1WI and 3D TOF MRA images. Our results demonstrate that the optimized 3D IR FSPGR sequence can potentially be used to replace the more traditional pre-contrast 2D T1WI technique in the detection of plaque hemorrhage and offer additional benefits of high-resolution volumetric visualization with 3D rendering.

2. Methods

2.1. Pulse sequence development and optimization

This sequence (Fig. 1) was developed by modifying the existing 3D IR FSPGR on a GE 3-T EXCITE scanner (GE Healthcare, Waukesha, WI, USA). The modifications include a 180° nonselective inversion recovery (IR) preparation RF pulse, an inclusion of fat signal saturation pulses on every encoding step and a sequential phase encoding strategy in the slice direction. The nonselective Silver–Hoult adiabatic inversion RF pulse provides a uniform inversion of spins even in the presence of a nonuniform B_1 field and inverts spins within the entire sensitive volume of the transmit coil [11]. By properly selecting the time of inversion (TI) based on the T_1 of the blood, the signal from the blood flow can be minimized to reach the maximum contrast between the carotid vessel lumen and the vessel wall. Fat saturation is applied on every data acquisition step to allow sufficient suppression of the fat signal. This is especially important when a surface coil is used. Selecting sequential phase encoding in the slice direction has provided good scan time efficiency. Since TI is equal to the time from the middle of the nonselective RF pulse to the acquisition RF pulse at the center of k-space in the slice direction, by properly selecting the number of slice phase encoding steps, the "dead" time $\mathrm{TI_{prep}}$ (the time from the middle of the nonselective inversion RF pulse to the middle of the RF pulse for the first encoding step) can be minimized.

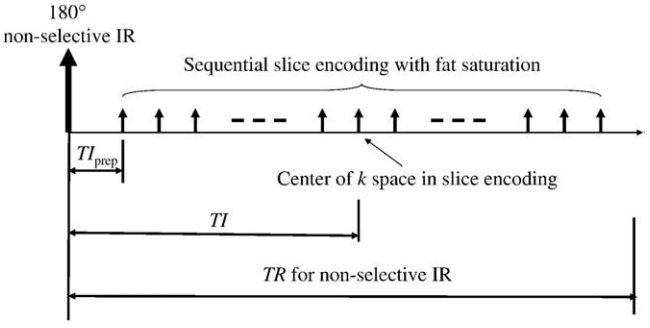

Fig. 1. Timing diagram of the optimized 3D IR FSPGR sequence.

The image signal acquired can be assessed based on computer simulations according to the basic design of the pulse sequence. The longitudinal magnetization $M_a(1)$ for the first slice encoding step is

$$M_a(1) = -M_{\text{before\_IR}} e^{-\frac{\text{TI}_{\text{prep}}}{T_1}} + M_0\left(1 - e^{-\frac{\text{TI}_{\text{prep}}}{T_1}}\right) \quad (1)$$

where M_0 is the longitudinal magnetization at a fully relaxed condition and can simply be modeled as 1 in simulation and $M_{\text{before\_IR}}$ is the longitudinal magnetization before the application of the 180° inversion RF pulse.

The longitudinal magnetizations for the second slice encoding step can be calculated and in the same manner for the subsequent slice encoding steps. The longitudinal magnetization $M_a(\text{i\_slice})$ for the slice phase encoding step i_slice is

$$M_a(\text{i\_slice}) = M_a(\text{i\_slice}-1)\cos(\alpha)e^{-\frac{\text{tr}}{T_1}} + M_0\left(1-e^{-\frac{\text{tr}}{T_1}}\right) \quad (2)$$

where α is the flip angle of the data acquisition pulse and tr is the time of repetition.

Lastly, the longitudinal magnetization before the application of the 180° inversion pulse is

$$M_{\text{before\_IR}} = M_a(\text{last\_slice})\cos(\alpha)e^{-\frac{t_{\text{extra}}}{T_1}} + M_0\left(1 - e^{-\frac{t_{\text{extra}}}{T_1}}\right) \quad (3)$$

where $M_a(\text{last\_slice})$ is the longitudinal magnetization for the last slice phase encoding step and t_{extra} is the time between the RF excitation of the last slice phase encoding step and the application of the 180° inversion pulse.

Instead of looking for an analytical solution for the image signal, a simulation can be used. The steady-state magnetization signal is achieved after a few iterations within the loop of Eqs. (1), then (2) and finally (3), with the initial $M_{\text{before\_IR}}$ set to 1. Ten iterations, which allowed the convergence to the steady state to the third significant digit, have been used in this paper. Since data is acquired with sequential slice encoding, the signal from the middle slice encoding step can be used to assess the image signal for a specific tissue type. Specifically,

$$M_{xy}(\text{i\_slice}) = M_z(\text{i\_slice})\sin(\alpha)e^{-\frac{\text{TE}}{T_2^*}} \quad (4)$$

where $M_{xy}(\text{i\_slice})$ is the transverse magnetization for slice phase encoding step i_slice.

The transverse magnetization is measured. A shortest possible TE (time of echo) based on the width limitations of the RF and gradient pulses has been chosen to minimize the T_2^* decay. For the purpose of the simulation, the T_2^* decay was ignored and the longitudinal magnetization was assumed to be the measured signal. The signals from different tissue types can be compared. For the simulation shown in Fig. 2,

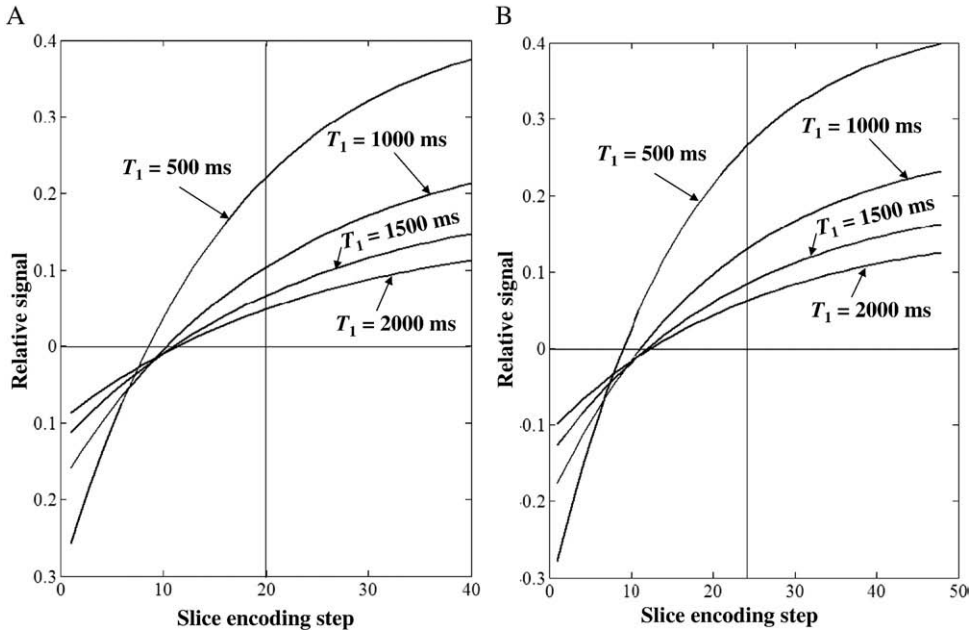

Fig. 2. Computer simulation of relative signal levels of four tissue types based on T_1 values of 500, 1000, 1500 and 2000 ms with TR=13.2 ms, TI_{prep}=40 ms, flip angle=15° and (A) number of slices=40 and (B) number of slices=48.

four hypothetical tissue types with T_1 values of 500, 1000, 1500 and 2000 ms are compared. Parameters of TR=13.2 ms, TI_{prep}=40 ms, flip angle=15° and number of slices=40 and 48 have been used in this simulation. Stanisz et al. [12] reported T_1 values of 1932±85 ms for blood, 1412±13 ms for skeletal muscle and 1471±31 ms for heart at 3 T. Noeske et al. [13] reported T_1 values of 1550±85 ms for blood and 1115±10 ms for myocardium at 3 T. It is reasonable to estimate that the T_1 of blood is within the range of 1500 to 2000 ms, and the T_1 of vessel wall is within the range of 1000 to 1500 ms at 3 T. Based on these numbers, both choices shown in Fig. 2 can provide reasonable levels of black-blood effect. Simulations with a flip angle of 10° were run again. Similar levels of black-blood effect were found. The other even more important consideration is that this technique needs to be highly sensitive to hemorrhage. T_1-shortening is one characteristic of hemorrhage both in the intracellular and extracellular methemoglobin state [10,14]. A hypothetical T_1 of 500 ms has been used in this simulation. Based on simulations, the contrast between the "hemorrhagic region" and "vessel wall" reduces with the increase of the data acquisition flip angle and the contrast reduction accelerates for flip angles greater than 25° and converges to a constant at a high flip angle (>30°). The simulation also shows that a range of scanning parameters can be used to achieve a reasonable imaging result that is sensitive to detect hemorrhage and to visualize the vessel wall. The simulations are instructive, but they are not definitive. Due to the relative uncertainty of the tissue T_1 values at the carotid region, the more optimized scanning parameters were acquired through volunteer studies, as demonstrated in the Results section.

The protocol with a total scan time of approximately 4 min has been used for collecting our subject data with a dedicated four-channel or six-channel carotid surface coil: TE=3.2 ms, the TR for each phase encoding step=13.2 ms, TI_{prep}=40 ms, flip angle=15°, receiver bandwidth=±31.25 kHz, field of view (FOV)=15 cm, slice thickness=1 mm, matrix size=256×192, number of excitation (NEX)=2 and number of slices=40 or 48 (which leads to TI=304 or 357 ms, and the TR with respect to the nonselective inversion=568 or 674 ms, respectively).

To compare with the 3D IR FSPGR, images have been acquired at the same slice locations with the T1WI and the 3D TOF MRA sequence. The T1WI were acquired using a fast spin-echo (FSE) sequence with the following scanning parameters: TR=800 ms, TE=11 ms, echo train length=10, receiver bandwidth=±20.8 kHz, FOV=16 cm, slice thickness=2 mm, number of slices=18, matrix size=256×256, phase FOV=0.8 and NEX=1. T_1-insensitive quadruple inversion-recovery (QIR) black-blood preparative sequence [15] (TI=520 ms) was used in combination with FSE for T1WI. The entire protocol included pre- and post-contrast T1WI scans. The 3D TOF images were acquired with the following scanning parameters: TR=23 ms, TE=3.9 ms, flip angle=20°, receiver bandwidth=±15.6 kHz, FOV=16 cm, slice thickness=1 mm, number of slices=48, matrix size=288×256 and NEX=1. The protocol also included T_2-weighted multi-slice double inversion-recovery [16] FSE sequence with the following parameters: TR=4000 ms, TE=50 ms, TI=250 ms, echo train length=12, receiver bandwidth=±15.63 kHz, FOV=16 cm, slice thickness=2 mm, number of slices=18, matrix size=256×256, phase FOV=0.75 and NEX=2. A contrast agent, gadobenate

dimeglumine (Gd-BOPTA, MultiHance; Bracco Diagnostic, Inc., Milan, Italy), was administered in a dose of 0.15 mmol/kg bodyweight, and post-contrast T1WI were acquired with the same parameters as pre-contrast T1WI.

The various plaque components were classified based upon criteria established by extensive prior research. The fibrous cap was described as thick, thin/absent or ruptured using previously described criteria on the bright-blood T_1-weighted images [17]. The presence and location of the lipid-rich necrotic core were measured by comparing black-blood T_1-weighted images pre- and post-contrast [18]. The presence and location of hemorrhage within the carotid plaque required review of the bright-blood T_1-weighted images, black blood T_1-weighted images as well as the black-blood T_2-weighted images [5]. Based upon prior work by Moody et al. [8] at 1.5 T, we anticipated that hemorrhage would appear bright at 3-T MR on our optimized 3D IR FSPGR images.

Regions of interest (ROI) were placed in the carotid plaque locations where hemorrhage was confirmed by histology. Additional ROI were placed in the adjacent sternocleidomastoid muscle and air. Both % contrast and CNR were calculated in the four plaques where intraplaque hemorrhage was detected. In the two remaining plaques, the ROIs were placed in the predominant plaque components (deep nonhemorrhagic necrotic core and dense fibrous region).

2.2. Subjects

One 28-year-old healthy female volunteer and six patients (four men, two women; mean age±S.D.=64±15 years; mean weight±S.D.=80±6 kg) scheduled for carotid endarterectomy participated in this study and signed consent forms approved by the Michigan State University Institutional Review Board. Data from the healthy volunteer was used to optimize the protocol and ensure effective blood suppression. The protocol was then applied to patient studies, with adjustments on the number of slices when larger coverage was needed. The carotid endarterectomy specimens from the six patients were sent to the Vascular Imaging Lab at the University of Washington for histological analysis and the results were compared with that from in vivo 3-T MR carotid plaque MR imaging.

3. Results

The 3D IR FSPGR protocol comparison was first performed on a healthy volunteer (Fig. 3). The effect of blood suppression was assessed based on the ratio (in percentage) of blood signal at the lumen vs. the tissue signal at the vessel wall. The comparison suggested that a minimum TI_{prep} should be used. Since the sequence was also intended to be optimized in terms of scan time efficiency, no extra relaxation time was given after the data acquisition. The protocol with 40 slice encoding steps showed the best contrast and the one with 48 slice encoding steps showed the second best contrast. Based on both healthy subjects and patients we have scanned, 36 mm of slab, equivalently 40 acquired slices at 1 mm slice thickness with our protocol, is about the minimum required to cover the carotid bifurcation and nearby regions. In some cases, 48 slices have been chosen to accommodate a better coverage. The black-blood effect decreased with the increase of the TI_{prep} for protocols with 40 or 48 slices, and thus the minimum TI_{prep} has been chosen.

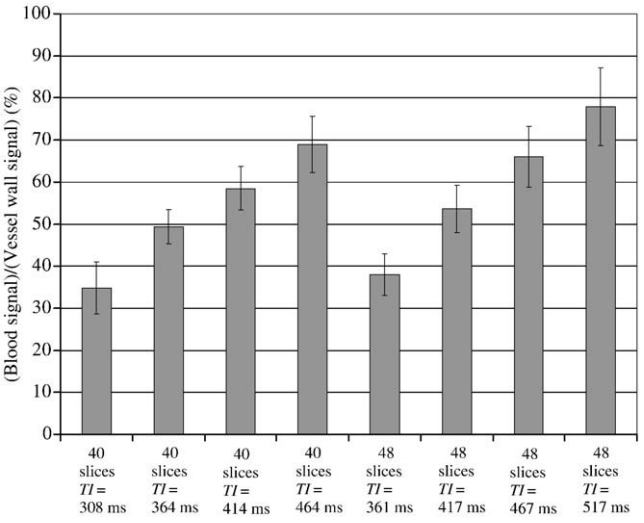

Fig. 3. Three-dimensional IR FSPGR protocol comparison on a normal volunteer. The effect of black blood is shown based on the % ratio of flowing blood signal in the lumen vs. signal at the vessel wall.

3.1. Subject summary

Table 1 lists the histology of the six patients participating in this study. The results from the optimized 3D IR FSPGR technique, the 2D QIR T_1-weighted and 3D TOF MRA are compared. Both the % contrast and the CNR are shown. In the four carotid plaques demonstrating hemorrhage on histological review of the CEA specimens, the % contrast and CNR are much higher with 3D IR FSPGR compared with 3D TOF MRA and 2D QIR T1WI in the corresponding hemorrhagic region noted on the preoperative in vivo 3-T MR study. In the remaining two carotid plaques with a predominately dense fibrous region and a necrotic core region noted on histological review, the % contrast and the CNR are comparable across the three imaging techniques on the in vivo 3-T MR carotid plaque study.

3.2. Case study 1: normal carotid artery

Images acquired with the optimized 3D IR FSPGR technique show clear blood and fat signal suppression at the carotid region (Fig. 4). This allows good visualization of the carotid lumen. Both the internal and external walls are well demarcated and are even better visualized through the coronal multiplanar reformation. The level of blood suppression can be compared with that achieved with the

Table 1
Imaging technique comparison of hemorrhagic plaque region

Subject number	Region of interest tissue type by histology	3D IR FSPGR		2D QIR T_1-weighted		3D TOF MRA	
		% Contrast	CNR	% Contrast	CNR	% Contrast	CNR
2	Fibrous plaque	−73.2	−26.8	−71.3	−32.9	−64.8	−46.9
4	Necrotic core	−63.5	−35.3	−51.1	−35.6	−64.7	−67.5
1	Hemorrhage	127.4	29.1	39.7	9.1	−14.0	−15.3
3	Hemorrhage	144.1	51.4	12.2	3.4	14.3	6.1
5	Hemorrhage	222.4	37.8	−8.0	−1.7	37.2	16.5
6	Hemorrhage	166.2	24.6	41.0	6.3	21.3	7.6

$$\%\ \text{Contrast} = \frac{(\text{Hemorrhage or plaque tissue mean signal intensity}) - (\text{Muscle mean signal intensity})}{\text{Muscle mean signal intensity}} \times 100\%$$

$$\text{CNR} = \frac{(\text{Hemorrhage or plaque tissue mean signal intensity}) - (\text{Muscle mean signal intensity})}{\text{Signal standard deviation at adjacent air}}$$

more traditional QIR T1WI (Fig. 4C) technique. The carotid lumen can also be readily visualized with the 3D TOF MRA images, but the boundary between the carotid lumen and vessel wall is less distinct.

3.3. Case study 2: carotid atherosclerotic plaque without hemorrhage

Images acquired with the optimized 3D IR FSPGR technique show clear delineation of the carotid plaque (Fig. 5). There is a focal region of decreased signal intensity that corresponds to a small necrotic core seen as a region of nonenhancement on the post-contrast QIR T1WI. This was confirmed on subsequent histological evaluation. No regions of high signal intensity were present on the 3D IR FSPGR to suggest plaque hemorrhage, and no regions of high signal within the carotid plaque on the QIR T1WI pre-contrast nor the 3D TOF MRA were noted. No plaque hemorrhage was identified on histology. High-quality multiplanar reformations of the 3D IR FSPGR data set are also possible and can aid in understanding the relationship of the plaque components with the lumen of the carotid bifurcation.

3.4. Case study 3: carotid atherosclerotic plaque with hemorrhage

Images acquired with the optimized 3D IR FSPGR technique show clear flowing blood and fat signal suppression at the carotid region with visualization of carotid lumen (Fig. 6). A hyper-intense hemorrhagic region within the carotid plaque was found with the optimized 3D IR FSPGR technique and confirmed later by histology. In this case, the boundaries of the hemorrhagic region on QIR T1WI and the 3D TOF MRA images were less distinct. The DIR T2WI indicates that this is an acute hemorrhage with a short T_2. The stage of hemorrhage was confirmed by histology.

4. Discussion

The role of plaque hemorrhage as a potential marker for symptomatic carotid plaque had been suggested as early as 1982 by Lusby et al. [4]. Their retrospective study of carotid endarterectomy specimens identified a significantly higher association of plaque hemorrhage in symptomatic patients when compared to asymptomatic patients. With the advent of in vivo MR plaque imaging, it is now possible to prospectively evaluate for plaque hemorrhage. One such study involved a total of 154 patients who were followed for a mean of 3 years after the initial in vivo carotid plaque study. In that study, plaque hemorrhage was shown to be statistically significantly associated with the development of new ipsilateral carotid stroke or transient ischemic attack in a prospective evaluation of asymptomatic patients with moderate carotid stenosis [19]. Altaf et al. [20] demonstrated increased incidence of recurrent ipsilateral carotid symptoms in patients waiting to undergo carotid endarterectomy when carotid plaque hemorrhage was detected by direct thrombus imaging (DTI) when compared to patients without hemorrhage. Patients with plaque hemorrhage demonstrated a more rapid increase in the size of the carotid plaques compared to those patients without hemorrhage when followed by longitudinal MRI

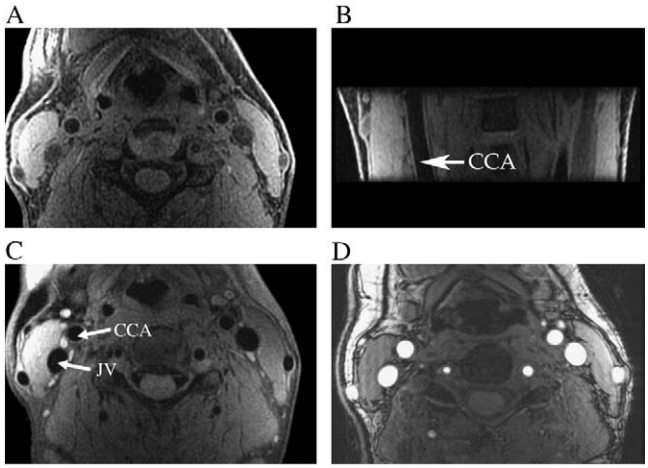

Fig. 4. Images acquired from a 28-year-old normal female volunteer with the optimized 3D IR FSPGR sequence are shown in the (A) axial and (B) coronal views. The images acquired with (C) a QIR T_1-weighted sequence and (D) a 3D TOF sequence at the same axial slice location are shown for comparison. (CCA=common carotid artery; JV=jugular vein.)

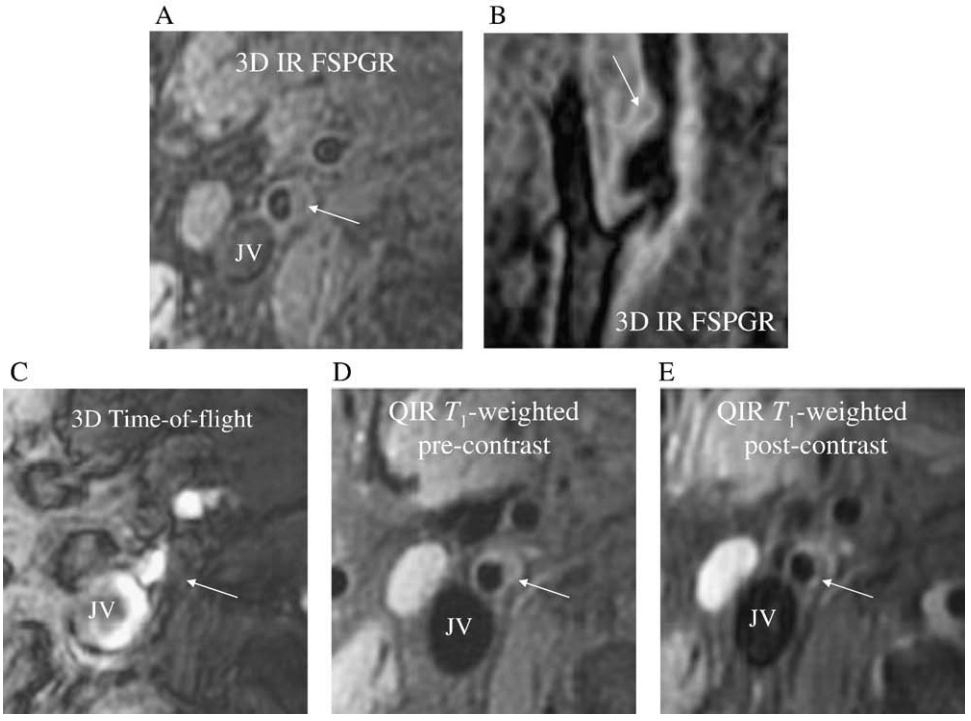

Fig. 5. Optimized 3D IR FSPGR images from a plaque without hemorrhage are shown in the (A) axial and (B) oblique sagittal multiplanar reformation. The images acquired with (C) 3D TOF MRA sequence, (D) pre-contrast QIR T_1-weighted sequence and (E) post-contrast QIR T_1-weighted sequence at the same axial slice location are shown for comparison. Note the small deep nonhemorrhagic necrotic core (confirmed at histology and indicated by arrows) in the wall of the right internal carotid artery.

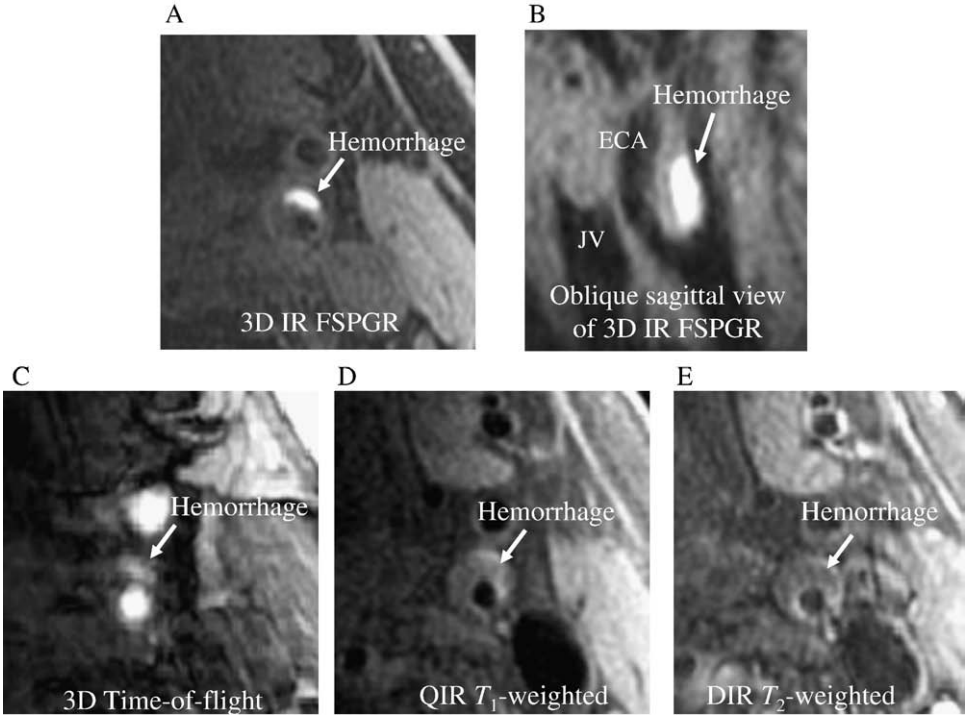

Fig. 6. Detection of hemorrhage through 3D IR FSPGR. The hemorrhagic region in the wall of the right internal carotid artery indicated by the arrow is shown in (A) axial view and (B) oblique sagittal multiplanar reformation. Images from (C) 3D TOF, (D) QIR T_1-weighted, and (E) DIR T_2-weighted acquisitions are shown for comparison. (ECA=external carotid artery.)

studies [21]. Ouhlous et al. [22] documented an increased number of white matter lesions when the carotid bifurcation contained hemorrhage.

We have developed a pulse sequence similar to the original DTI sequence proposed by Moody et al. [8], but optimized for 3 T. When the optimized 3D IR FSPGR sequence is combined with dedicated carotid coil imaging at 3 T, it is possible to achieve high spatial resolution (approximately 0.7 mm in-plane resolution) with sufficient coverage to visualize both carotid bifurcations in under 5 min. The optimized 3D IR FSPGR highlights plaque hemorrhage by providing higher % contrast and CNR compared with 2D T1WI and 3D TOF MRA. There were some inter-subject variations in the level of the black-blood effect due to in-flow issue, but the high % contrast between the hemorrhagic and the surrounding regions was maintained. The potential for improved sensitivity and specificity in the detection of hemorrhage by recently trained radiologists using the higher CNR 3D IR FSPGR compared to 3D TOF MRA and 2D QIR T1WI is currently under study.

The optimized 3D IR FSPGR provides similar contrast levels as 2D T1WI in nonhemorrhagic plaque regions. The 3D IR FSPGR images can also provide high-quality multiplanar reformations for localizing the abnormal regions. However, the 2D T1WI provides higher signal-to-noise ratio, which allows a better depiction of the vessel wall. A more detailed comparison within a larger patient population utilizing 3D IR FSPGR with T1WI and 3D TOF MRA using histological validation is currently ongoing. Single-echo 3D IR FSPGR sequence cannot differentiate Type I and Type II hemorrhages. A multi-echo 3D IR FSPGR sequence is under development and may be able to achieve high sensitivity and specificity for plaque hemorrhage detection while at the same time characterizing the age of the hemorrhage.

Acknowledgment

The authors thank Dr. Vasily Yarnykh for providing the original QIR T_1-weighted and DIR T_2-weighted sequence source codes, and Ms. Colleen Hammond for scanning support.

References

[1] Yuan C, Kerwin WS. MRI of atherosclerosis. J Magn Reson Imaging 2004;19:710–9.
[2] Shah PK. Mechanisms of plaque vulnerability and rupture. J Am Coll Cardiol 2003;41:15S–22S.
[3] Fryer JA, Myers PC, Appleberg M. Carotid intraplaque hemorrhage: the significance of neovascularity. J Vasc Surg 1987;6:341–9.
[4] Lusby RJ, Ferrell LD, Ehrenfeld WK, Stoney RJ, Wylie EJ. Carotid plaque hemorrhage. Its role in production of cerebral ischemia. Arch Surg 1982;117:1479–88.
[5] Chu B, Kampschulte A, Ferguson MS, et al. Hemorrhage in the atherosclerotic carotid plaque: a high-resolution MRI study. Stroke 2004;35:1079–84.
[6] Kampschulte A, Ferguson MS, Kerwin WS, et al. Differentiation of intraplaque versus juxtaluminal hemorrhage/thrombus in advanced human carotid atherosclerotic lesions by in vivo magnetic resonance imaging. Circulation 2004;110:3239–44.
[7] Saam T, Cai J, Ma L, et al. Comparison of symptomatic and asymptomatic atherosclerotic carotid plaque features with in vivo MR imaging. Radiology 2006;240:464–72.
[8] Moody AR, Murphy RE, Morgan PS, et al. Characterization of complicated carotid plaque with magnetic resonance direct thrombus imaging in patients with cerebral ischemia. Circulation 2003;107:3047–52.
[9] Yarnykh VL, Terashima M, Hayes CE, et al. Multicontrast black-blood MRI of carotid arteries: comparison between 1.5 and 3 tesla magnetic field strengths. J Magn Reson Imaging 2006;23:691–8.
[10] Allkemper T, Tombach B, Schwindt W, et al. Acute and subacute intracerebral hemorrhages: comparison of MR imaging at 1.5 and 3.0 T — initial experience. Radiology 2004;232:874–81.
[11] Silver M, Joseph R, Hoult D. Highly selective π/2 and π pulse generation. J Magn Reson 1984;59:347–51.
[12] Stanisz GJ, Odrobina EE, Pun J, et al. T1, T2 relaxation and magnetization transfer in tissue at 3T. Magn Reson Med 2005;54:507–12.
[13] Noeske R, Seifert F, Rhein KH, Rinneberg H. Human cardiac imaging at 3 T using phased array coils. Magn Reson Med 2000;44:978–82.
[14] Gomori JM, Grossman RI. Mechanisms responsible for the MR appearance and evolution of intracranial hemorrhage. Radiographics 1988;8:427–40.
[15] Yarnykh VL, Yuan C. T1-insensitive flow suppression using quadruple inversion-recovery. Magn Reson Med 2002;48:899–905.
[16] Yarnykh VL, Yuan C. Multislice double inversion-recovery black-blood imaging with simultaneous slice reinversion. J Magn Reson Imaging 2003;17:478–83.
[17] Hatsukami TS, Ross R, Polissar NL, Yuan C. Visualization of fibrous cap thickness and rupture in human atherosclerotic carotid plaque in vivo with high-resolution magnetic resonance imaging. Circulation 2000;102:959–64.
[18] Yuan C, Kerwin WS, Ferguson MS, et al. Contrast-enhanced high resolution MRI for atherosclerotic carotid artery tissue characterization. J Magn Reson Imaging 2002;15:62–7.
[19] Takaya N, Yuan C, Chu B, et al. Association between carotid plaque characteristics and subsequent ischemic cerebrovascular events: a prospective assessment with MRI — initial results. Stroke 2006;37:818–23.
[20] Altaf N, MacSweeney ST, Gladman J, Auer DP. Carotid intraplaque hemorrhage predicts recurrent symptoms in patients with high-grade carotid stenosis. Stroke 2007;38:1633–5.
[21] Takaya N, Yuan C, Chu B, et al. Presence of intraplaque hemorrhage stimulates progression of carotid atherosclerotic plaques: a high-resolution magnetic resonance imaging study. Circulation 2005;111:2768–75.
[22] Ouhlous M, Flack H, de Weert T, et al. Carotid plaque composition and cerebral infarction: MR imaging study. Am J Neuroradiol 2005;26:1044–9.